

Search for $WW\gamma$ and $WZ\gamma$ Production, and Anomalous
Quartic Gauge Couplings in pp collisions at CMS/LHCPATRICIA REBELLO TELES¹
ON BEHALF OF CMS COLLABORATION*Centro Brasileiro de Pesquisas Físicas – CBPF
Rua Dr. Xavier Sigaud 150, 22290-180, Rio de Janeiro, RJ, Brasil**LHC Physics Center
Fermi National Accelerator Laboratory, Batavia, IL 60510**E-mail: patricia.rebello.teles@cern.ch*

Based on a talk given at the APS DPF 2013, this proceedings deals with the study of the three gauge boson $WV\gamma$ production, containing a W boson decaying leptonically, a second V (W^\pm or Z) boson decaying to two jets, and a photon γ , and the anomalous quartic gauge boson couplings taking into account the data collected by CMS detector at the Large Hadron Collider in 2012 at $\sqrt{s}=8$ TeV with integrated luminosity of 19.3 fb^{-1} .

PRESENTED AT

DPF 2013

The Meeting of the American Physical Society
Division of Particles and Fields
Santa Cruz, California, August 13–17, 2013

¹Work supported by Conselho Nacional de Desenvolvimento Científico e Tecnológico (CNPq) and LHC Physics Center (LPC)

1 Introduction

Aiming to observe the three gauge boson production by extending the precisely measured diboson production analysis at CMS [1, 2] with energetic photons, in order to model the electromagnetic radiation in the WW and WZ pair creation processes, we notice that these channels are also suitable for the SM quartic interactions as well as sensitive to deviations of them.

Due to its non-abelian $SU(2)_L \otimes U(1)_Y$ gauge symmetry structure, from the SM naturally emerges the quartic $WWWW$, $WWZZ$, $WWZ\gamma$ and $WW\gamma\gamma$ vertices. The investigation of them is expected to play an important role at LHC energies, mainly because they have a great potential to explore possible new physics expressed in a model independent way by high-dimensional effective operators [3] leading to anomalous quartic gauge couplings (aQGC). Recently the anomalous $WW\gamma\gamma$ vertex was constrained through the exclusive WW production [4].

This analysis [5] is focused on $WV\gamma$ production in the semi-leptonic final state which includes $W(\rightarrow l\nu_l)W(\rightarrow jj)\gamma$ and $W(\rightarrow l\nu_l)Z(\rightarrow jj)\gamma$ processes and was chosen due to the higher branching ratio compared to the fully leptonic mode. Since these two production reactions cannot be differentiated due to the detector di-jet mass resolution close to the mass difference between W and Z bosons, and the semi-leptonic final state has a common dominant background, that is $W(\rightarrow l\nu_l)\gamma + \text{jets}$, then we have treated both channels as combined signal in this analysis.

2 Theory

Anomalous vertices may be associated either to dimension 6 or to dimension 8 effective operators, which emerge naturally from convenient gauge symmetry realizations in a model independent way [3].

Concerning the anomalous quartic vertices involving photons, as $WW\gamma\gamma$ and $WWZ\gamma$, the effective operators tested in this analysis can be written as

$$\mathcal{L}_{AQGC} = \frac{a_0^W}{4g^2} \mathcal{W}_0^\gamma + \frac{a_c^W}{4g^2} \mathcal{W}_c^\gamma + \sum_i k_i^W \mathcal{W}_i^Z + \mathcal{L}_{T,0} \quad (1)$$

where the dimension 6, $a_{0,C}^W$ and $\kappa_{0,C}^W$, parameters are associated with the $WW\gamma\gamma$ and $WWZ\gamma$ vertices respectively, while the parameter $f_{T,0}$, from $L_{T,0}$ dimension 8 operator, is associated with both.

Moreover, some dimension 6 and dimension 8 operators are similar, as we can see at Fig. 1, and can be related through the linear transformations

$$\frac{f_{M0}}{\Lambda^4} = \frac{g^2}{4M_W^4 s_W^2} \frac{k_0^w}{\Lambda^2}, \quad \frac{f_{M2}}{\Lambda^4} = \frac{g'^2}{2M_W^4 s_W^2} \frac{k_0^b}{\Lambda^2}, \quad \frac{f_{M1}}{\Lambda^4} = \frac{g^2}{2M_W^4 s_W^2} \frac{k_C^w}{\Lambda^2}, \quad \frac{f_{M3}}{\Lambda^4} = \frac{g'^2}{M_W^4 s_W^2} \frac{k_C^b}{\Lambda^2}$$

being also valid the relation

$$a_{0,C}^W = 4g^2(k_{0,C}^w + k_{0,C}^b + k_{0,C}^m).$$

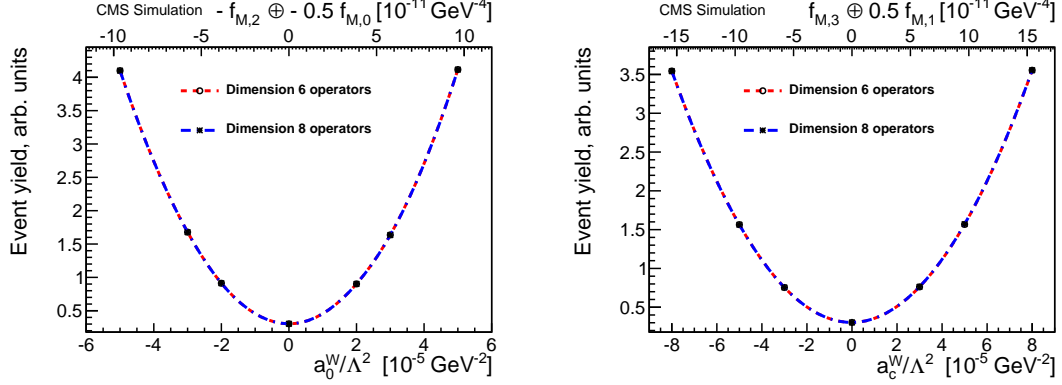


Figure 1: Dimension 8 parameters $f_{M,i}$ can be associated to dimension 6 $a_{0,C}^W$ through simple linear transformations.

3 Selection Criteria and Simulation

For the SM $WV\gamma$ search, a cut and count approach was adopted, based on the selection criteria described here.

We have used MADGRAPH 5.1.3.22 [6], adopting CTEQ6L1 as parton distribution function, to generate leading order (LO) events samples for signal and backgrounds. Single top samples were generated with POWHEG [6]. A summary of the contributing processes is given in Table 1.

All LO samples were matched to parton showers from PYTHIA 6.426 [7]. To derive the corresponding K-factors for three boson production ($K_{WV\gamma} = 2.1$) and aQGC ($K_{aQGC} = 1.2$) we have used de aMC@NLO [6]. For each aQGC parameter, several samples were generated with different values of the parameters, maintaining all other parameters equal to zero.

The leptonic W gauge boson includes a requirement of transverse mass ($M_T^W > 30$ GeV), with either one electron ($E_T^e > 30$ GeV, $|\eta^e| < 2.5$, excluding $1.44 < |\eta^e| < 1.57$) or one muon ($p_T^\mu > 25$ GeV, $|\eta^\mu| < 2.1$) in the final state. Events with additional leptons are vetoed to reduce backgrounds with di- and tri-lepton final states. The neutrino induces a selection requirement of $E_T > 35$ GeV.

The two most energetic jet candidates are required to satisfy $p_T^j > 30$ GeV and $|\eta^j| < 2.4$. The photon candidate must satisfy $E_T^\gamma > 30$ GeV and $|\eta^\gamma| < 1.44$. The

Process	shape modeling	cross section[pb]
SM $WW\gamma$	MC	(NLO) 0.0896 ± 0.0213
SM $WZ\gamma$	MC	(NLO) 0.0121 ± 0.0029
$W\gamma$ +Jets	MC	(data) 10.872 ± 0.087
jet $\rightarrow \gamma$	data	data
$Z\gamma$ +Jets	MC	(LO) 0.632 ± 0.126
$t\bar{t}\gamma$	MC	(LO) 0.615 ± 0.123
Single Top + γ (inclusive)	MC	(NLO) 0.310 ± 0.011

Table 1: Summary of the SM processes adopted in this analysis. NLO cross section assuming $p_T^\gamma > 10$ GeV and $|\eta^\gamma| < 2.5$

data were collected with single-lepton triggers using p_T thresholds of 24-30 GeV for muons and 27-32 GeV for electrons.

The azimuthal separation $\Delta\phi$ between the leading jet and the \cancel{E}_T direction, have to be larger than 0.4 to reduce mismeasured \cancel{E}_T . To reduce $W\gamma$ +jets background events, a di-jet invariant mass window of $70 < m_{jj} < 100$ GeV, and a separation between the jets of $|\Delta\eta_{jj}| < 1.4$, were imposed. More details, as well as a summary of all the contributing systematics uncertainties, is given at [5].

4 Results

4.1 SM $WV\gamma$ Cross Section

The $WW\gamma$ and $WZ\gamma$ cross section measurement in pp collisions at $\sqrt{s}=8$ TeV is not accessible with the data collected in 2012 by the CMS detector due low statistics. In fact, after the cut & count approach based on selection criteria described before we have observed 322 events observed (See Table 2) against 341.5 ± 15.8 events predicted (See Table 1).

Therefore it was only possible to set a one-sided upper limit on the cross section. For the amount of data presented here, we have set an upper limit of 0.24 pb at 95% C.L. for $WV\gamma$ with photon $p_T > 10$ GeV, which corresponds to 3.4 times the SM prediction.

4.2 Exclusion Limits for the Anomalous Quartic Gauge Couplings

The photon p_T distributions, segregated by lepton flavor, was used after all selection criteria as the observable to set limits on the aQGC parameters. See Fig. 2 which

Process	muon channel number of events	electron channel number of events
W γ +jets	$136.9 \pm 3.5 \pm 9.2 \pm 0.0$	$101.6 \pm 2.9 \pm 8.0 \pm 0.0$
WV+jet, jet $\rightarrow\gamma$	$33.1 \pm 1.3 \pm 4.6 \pm 0.0$	$21.3 \pm 1.0 \pm 3.1 \pm 0.0$
MC $t\bar{t}\gamma$	$12.5 \pm 0.8 \pm 2.9 \pm 0.3$	$9.1 \pm 0.7 \pm 2.1 \pm 0.2$
MC single top	$2.8 \pm 0.8 \pm 0.2 \pm 0.1$	$1.7 \pm 0.6 \pm 0.1 \pm 0.0$
MC Z γ +jets	$1.7 \pm 0.1 \pm 0.1 \pm 0.0$	$1.5 \pm 0.1 \pm 0.1 \pm 0.0$
multijets	$<0.2 \pm 0.0 \pm 0.1 \pm 0.0$	$7.2 \pm 3.6 \pm 3.6 \pm 0.0$
SM WW γ	$6.6 \pm 0.1 \pm 1.5 \pm 0.2$	$5.0 \pm 0.1 \pm 1.1 \pm 0.1$
SM WZ γ	$0.6 \pm 0.0 \pm 0.1 \pm 0.0$	$0.5 \pm 0.0 \pm 0.1 \pm 0.0$
Total predicted	$194.2 \pm 3.9 \pm 10.8 \pm 0.6$	$147.9 \pm 4.8 \pm 9.6 \pm 0.4$
Data	183	139

Table 2: Expected number of events per process, with statistical, systematic and luminosity uncertainties quoted.

Observed Limits	Expected Limits
$-21 \text{ (TeV}^{-2}) < a_0^W/\Lambda^2 < 20 \text{ (TeV}^{-2})$	$-24 \text{ (TeV}^{-2}) < a_0^W/\Lambda^2 < 23 \text{ (TeV}^{-2})$
$-34 \text{ (TeV}^{-2}) < a_C^W/\Lambda^2 < 32 \text{ (TeV}^{-2})$	$-37 \text{ (TeV}^{-2}) < a_C^W/\Lambda^2 < 34 \text{ (TeV}^{-2})$
$-25 \text{ (TeV}^{-4}) < f_{T,0}/\Lambda^4 < 24 \text{ (TeV}^{-4})$	$-27 \text{ (TeV}^{-4}) < f_{T,0}/\Lambda^4 < 27 \text{ (TeV}^{-4})$
$-12 \text{ (TeV}^{-2}) < \kappa_0^W/\Lambda^2 < 10 \text{ (TeV}^{-2})$	$-12 \text{ (TeV}^{-2}) < \kappa_0^W/\Lambda^2 < 12 \text{ (TeV}^{-2})$
$-18 \text{ (TeV}^{-2}) < \kappa_C^W/\Lambda^2 < 17 \text{ (TeV}^{-2})$	$-19 \text{ (TeV}^{-2}) < \kappa_C^W/\Lambda^2 < 18 \text{ (TeV}^{-2})$

Table 3: 95% C.L. shape-based exclusion limits listed for both the muon and electron channels of each aQGC parameter using photon p_T .

show the excess of events profile for the muon channel for given values of aQGC parameters.

Finally, no evidence of anomalous $WW\gamma\gamma$ and $WWZ\gamma$ quartic gauge couplings was found and we have computed exclusion limits (See Tables 3 and 4) for the several aQGC parameters at the 95% C.L.

A small asymmetry in the limits is expected due to the interference between the SM and aQGC processes. These are the first ever limits on dimension 8 $f_{T,0}$ and dimension 6 CP-conserving couplings $\kappa_{0,C}^W$.

A comparison of several existing limits on the $WW\gamma\gamma$ aQGC parameter is shown on Figure 3. The CMS limits are orders of magnitude more stringent than the best limits obtained at LEP and Tevatron.

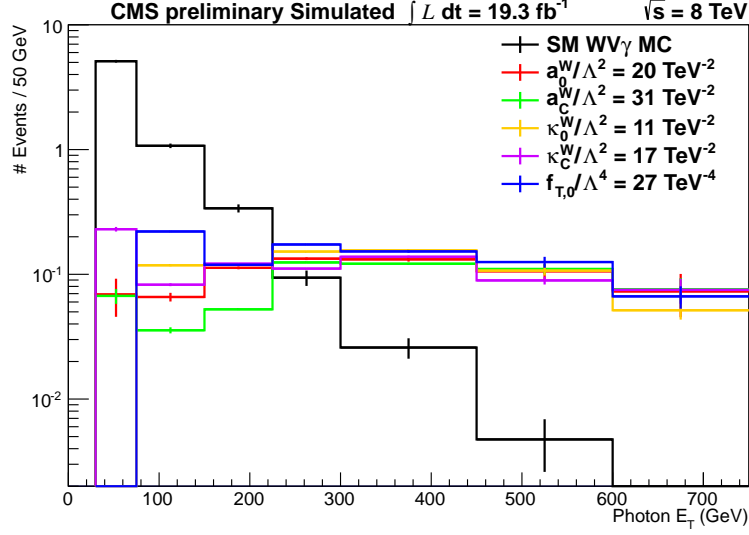


Figure 2: Plot of photon E_T distributions after all selections for the muon channel for the SM prediction and for the aQGC signals for the five parameters. The distributions are similar for the electron channel.

Observed Limits	Expected Limits
$-77 \text{ (TeV}^{-4}\text{)} < f_{M,0}/\Lambda^4 < 81 \text{ (TeV}^{-4}\text{)}$	$-89 \text{ (TeV}^{-4}\text{)} < f_{M,0}/\Lambda^4 < 93 \text{ (TeV}^{-4}\text{)}$
$-131 \text{ (TeV}^{-4}\text{)} < f_{M,1}/\Lambda^4 < 123 \text{ (TeV}^{-4}\text{)}$	$-143 \text{ (TeV}^{-4}\text{)} < f_{M,1}/\Lambda^4 < 131 \text{ (TeV}^{-4}\text{)}$
$-39 \text{ (TeV}^{-4}\text{)} < f_{M,2}/\Lambda^4 < 40 \text{ (TeV}^{-4}\text{)}$	$-44 \text{ (TeV}^{-4}\text{)} < f_{M,2}/\Lambda^4 < 46 \text{ (TeV}^{-4}\text{)}$
$-66 \text{ (TeV}^{-4}\text{)} < f_{M,3}/\Lambda^4 < 62 \text{ (TeV}^{-4}\text{)}$	$-71 \text{ (TeV}^{-4}\text{)} < f_{M,3}/\Lambda^4 < 66 \text{ (TeV}^{-4}\text{)}$

Table 4: 95% C.L. shape-based exclusion limits listed for both the muon and electron channels of each dimension 8 aQGC parameter, using photon PT as the observable.

Acknowledgments

The author is deeply grateful to LPC Physics Center for the hospitality and support during the essential steps of this investigation.

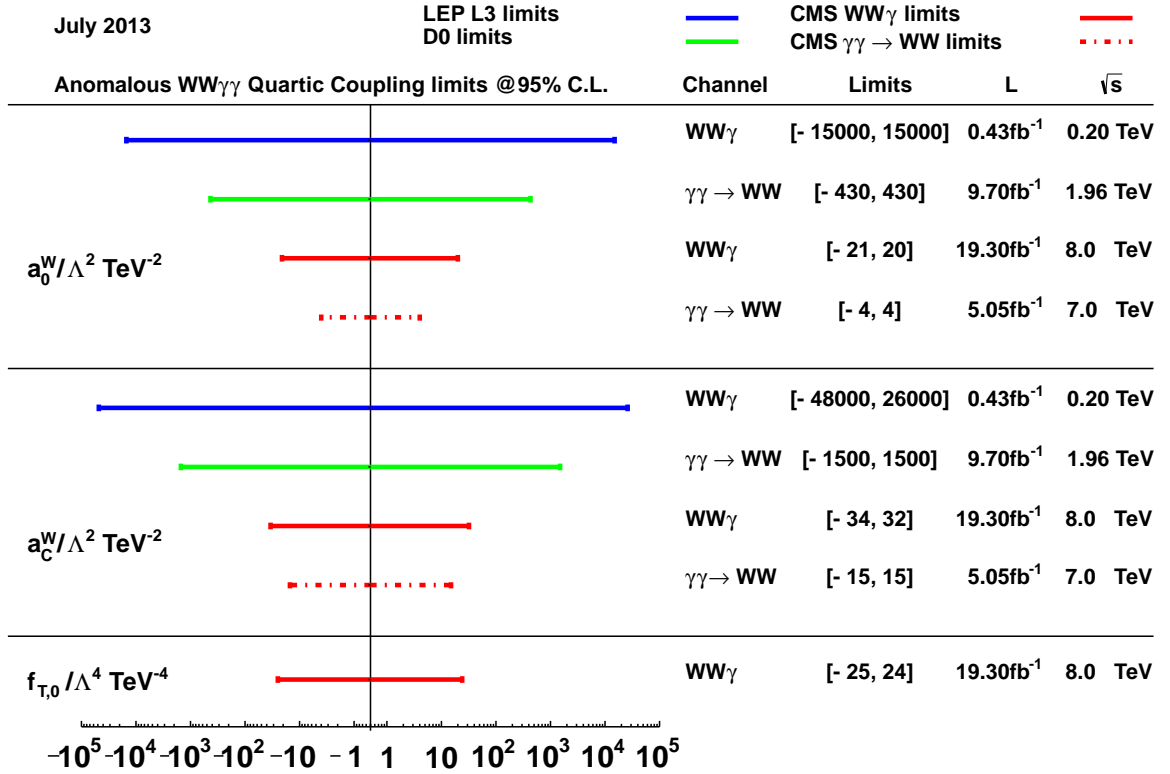


Figure 3: Plot comparing the previous limits with limits from LEP, Tevatron, and other CMS measurements.

References

- [1] CMS Collaboration, JINST **3**, S08004 (2008).
- [2] CMS Collaboration, Eur. Phys. J. Sci. **C73**, 2283 (2013).
- [3] G. Belanger and F. Boudjema, Phys. Lett. **B288**, 201 (1992), Eur. Phys. J. **C13**, 283 (2000); O. Eboli et al., Phys. Rev. **D69**, 095005 (2004); O. Eboli et al., Phys. Rev. **D74**, 073005 (2006); D. Yang et al., JHEP **1304**, 108 (2013).
- [4] CMS Collaboration, JHEP **07**, 116 (2013).
- [5] CMS Collaboration, CMS-PAS-SMP-13-009, <https://twiki.cern.ch/twiki/bin/view/CMSPublic/PhysicsResultsSMP13009>.
- [6] J. Alwall et al., JHEP **1106**, 128 (2011); E. Re, Eur. Phys. J. **C71** 1547 (2011); S. Frixione and B. R. Webber, JHEP **0206**, 029 (2006).
- [7] T. Sjostrand et al., JHEP **05**, 026 (2006).